ACCOUNTS of chemical research

Article

Cite This: Acc. Chem. Res. 2018, 51, 2906−2917

pubs.acs.org/accounts

# Structure- and Electrolyte-Sensitivity in $CO_2$ Electroreduction

Rosa M. Arán-Ais,[†,‡,§] Dunfeng Gao,[†,‡,§] and Beatriz Roldan Cuenya*[,‡]

[†]Department of Physics, Ruhr-University Bochum, 44780 Bochum, Germany

[‡]Department of Interface Science, Fritz-Haber-Institute of the Max Planck Society, 14195 Berlin, Germany

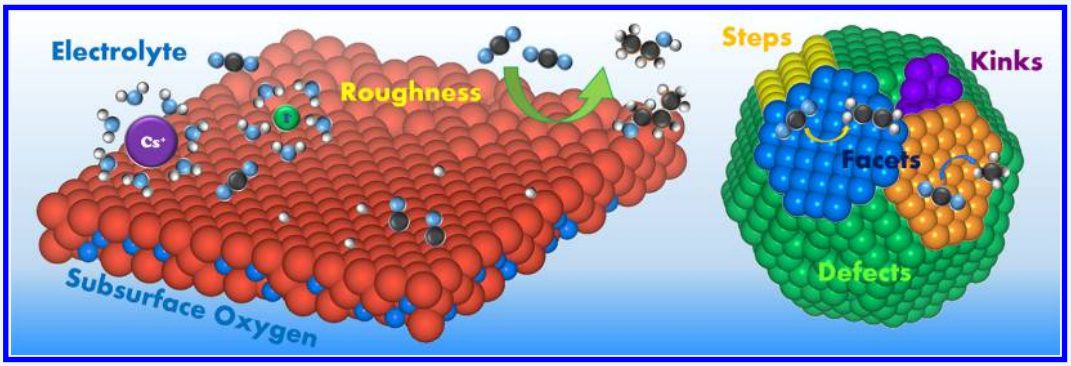


**ABSTRACT:** The utilization of fossil fuels (i.e., coal, petroleum, and natural gas) as the main energy source gives rise to serious environmental issues, including global warming caused by the continuously increasing level of atmospheric $CO_2$. To deal with this challenge, fossil fuels are being partially replaced by renewable energy such as solar and wind. However, such energy sources are usually intermittent and currently constitute a very low portion of the overall energy consumption. Recently, the electrochemical conversion of $CO_2$ to chemicals and fuels with high energy density driven by electricity derived from renewable energy has been recognized as a promising strategy toward sustainable energy.

The activation and reduction of $CO_2$, which is a thermodynamically stable and kinetically inert molecule, is extremely challenging. Although the participation of protons in the $CO_2$ electroreduction reaction ($CO_2$RR) helps lower the energy barrier, high overpotentials are still needed to efficiently drive the process. On the other hand, the concurrent hydrogen evolution reaction (HER) under $CO_2$RR conditions leads to lower selectivity toward $CO_2$RR products. Electrocatalysts that are highly active and selective for multicarbon products are urgently needed to improve the energy efficiency of $CO_2$RR. The reduction of $CO_2$ involves multiple proton−electron transfers and has many complex intermediates. Recent reports have shown that the relative stability of the intermediates on the surface of catalysts determines final reaction pathways as well as the product selectivity. Furthermore, this reaction displays a strong structure-sensitivity. The atomic arrangement, electronic structure, chemical composition, and oxidation state of the catalysts significantly influence catalyst performance. Fundamental understanding of the dependence of the reaction mechanisms on the catalyst structure would guide the rational design of new nanostructured $CO_2$RR catalysts. As a reaction proceeding in a complex environment containing gas/liquid/solid interfaces, $CO_2$RR is also intensively affected by the *electrolyte*. The electrolyte composition in the near surface region of the electrode where the reaction takes place plays a vital role in the reactivity. However, the former might also be indirectly determined by the bulk electrolyte composition via diffusion. Adding to the complexity, the structure, chemical state and surface composition of the catalysts under reaction conditions usually undergo dynamic changes, especially when adsorbed ions are considered. Therefore, in addition to tuning the structure of the electrocatalysts, being able to also modify the electrolyte provides an alternative method to tune the activity and selectivity of $CO_2$RR. In situ and operando characterization methods must be employed to gain in depth understanding on the structure- and electrolyte-sensitivity of real $CO_2$RR catalysts under working conditions.

This Account provides examples of recent advances in the development of nanostructured catalysts and mechanistic understanding of $CO_2$RR. It discusses how the structure of a catalyst (crystal orientation, oxidation state, atomic arrangement, defects, size, surface composition, segregation, etc.) influences the activity and selectivity, and how the electrolyte also plays a determining role in the reaction activity and selectivity. Finally, the importance of in situ and operando characterization methods to understand the structure- and electrolyte-sensitivity of the $CO_2$RR is discussed.

## 1. INTRODUCTION

The electrochemical conversion of $CO_2$ provides a potential solution to address some of the future energy needs by converting greenhouse gases into valuable fuels or feedstocks. The use of renewable energy sources to supply the electrons needed to electroreduce $CO_2$ makes this process attractive, so that the intermittent electricity coming from solar, wind, or

Received: July 20, 2018
Published: October 18, 2018






DOI: 10.1021/acs.accounts.8b00360
Acc. Chem. Res. 2018, 51, 2906−2917

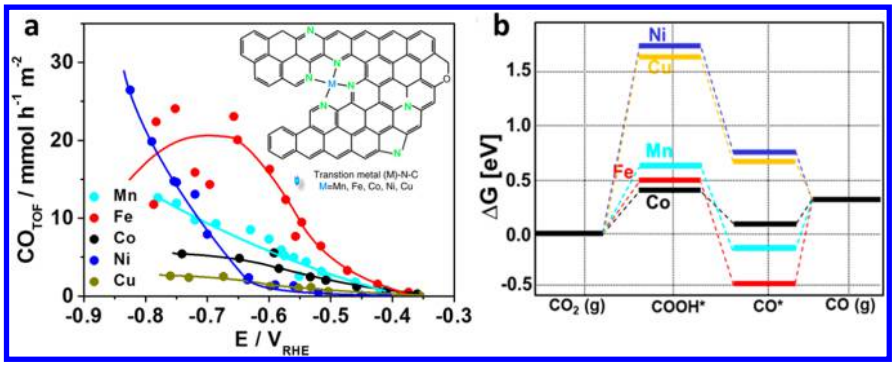


**Figure 1.** (a) CO production rate of M−N−C catalysts versus potential. Inset: schematic structure of the M−N−C catalysts. (b) Free energy diagrams of $CO_2$RR at −0.8 $V_{RHE}$ for M−N−C catalysts. Reproduced with permission from ref 4. Copyright 2017 Nature Publishing Group.

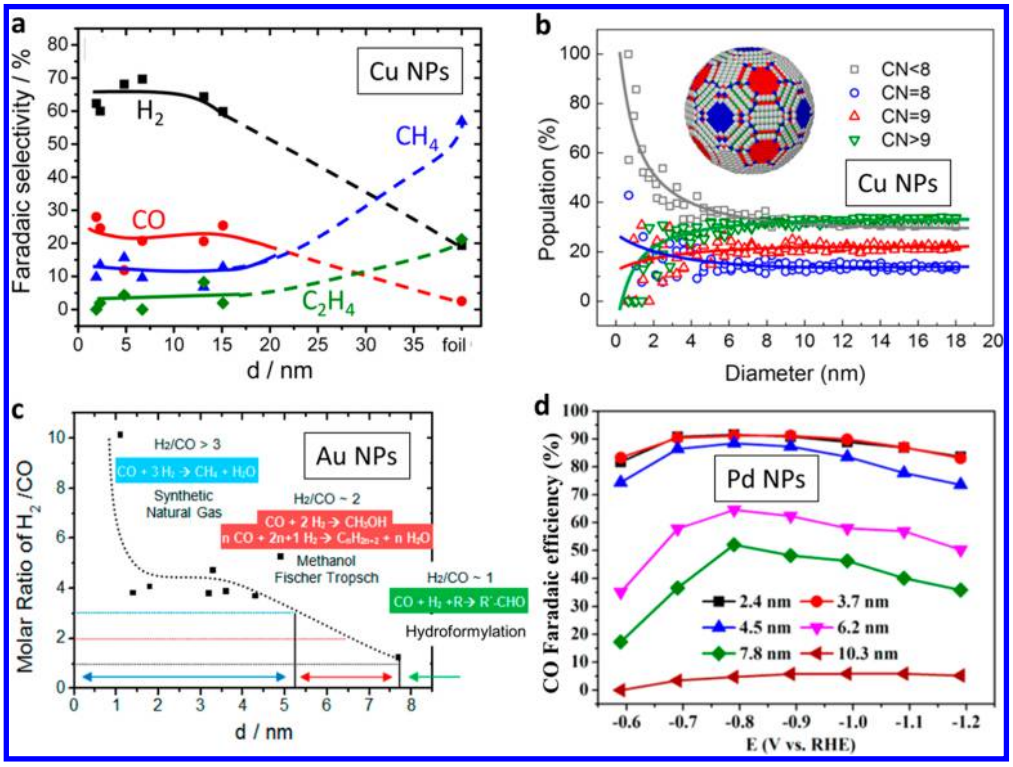


**Figure 2.** (a) Faradaic selectivity and (b) population of specifically coordinated surface atoms as a function of Cu NP size. Reproduced with permission from ref 8. Copyright 2014 American Chemical Society. (c) Molar ratio of $H_2$ and CO produced at −1.2 $V_{RHE}$ as a function of NP size. Reproduced with permission from ref 10. Copyright 2014 American Chemical Society. (d) CO FE of Pd NPs with different sizes. Reproduced with permission from ref 11. Copyright 2015 American Chemical Society.

hydro-power technologies could be complemented by the energy stored in the chemical bonds of high-energy-density products coming from captured $CO_2$. However, this molecule is extremely stable, being the $CO_2$ electroreduction reaction ($CO_2$RR) an uphill process that requires high overpotentials and presents numerous other challenges. The multiple proton-electron transfer steps required to reduce $CO_2$ into fuels, accompanied by the competing hydrogen evolution reaction (HER), leads to poor selectivity toward multicarbon compounds (e.g., ethylene and ethanol). The later species and other so-called $C_{2+}$ products are highly sought because of their higher value, greater energy density, and broader applicability than $C_1$ products. Therefore, the development of highly active and selective catalysts, as well as an optimum technology that improves the effective $CO_2$ conversion, are key challenges for practical application of the $CO_2$RR.

Among all metals, Cu is the only metal capable of efficiently reducing $CO_2$ to hydrocarbons and alcohols, while hydrogen, CO, and formate are the major products produced by other metals.[1] The $CO_2$RR is a *structure-sensitive process*, meaning that the atomic arrangement at the catalyst surface affects the adsorption and bond cleavage of the reactants, thus determining the catalytic performance. Recent reports have opened new perspectives in exploring both compositional and morphological effects toward the rational design of more selective catalysts. Moreover, optimizing the reaction environment has also been demonstrated to be critical to address some of the challenges of this reaction, such as the low solubility of $CO_2$, changes in pH, and stabilization of certain active species.

In this Account, we provide an overview of the current understanding of the $CO_2$RR, focusing on the strategies followed so far for the development of more efficient and


DOI: 10.1021/acs.accounts.8b00360
Acc. Chem. Res. 2018, 51, 2906−2917

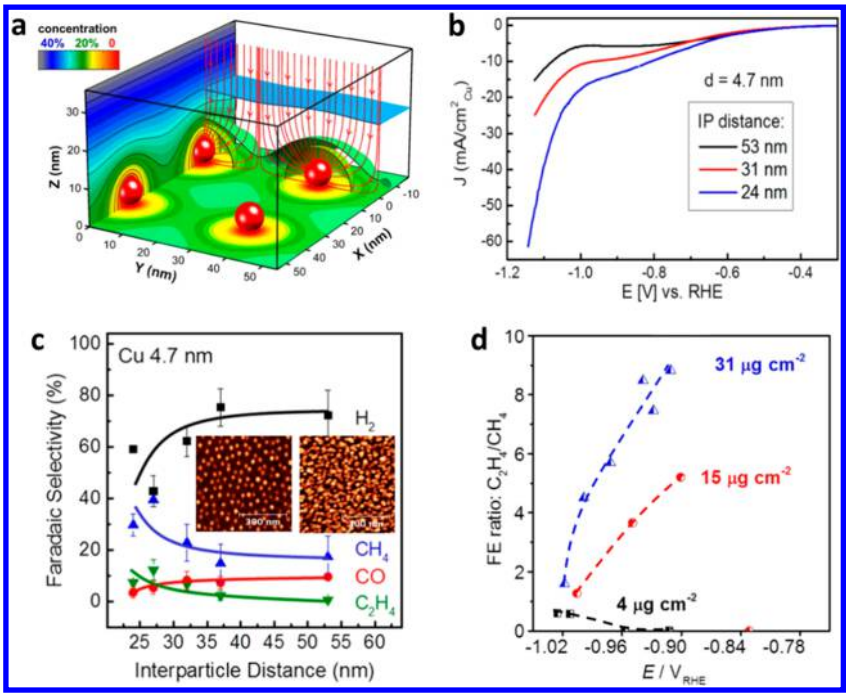


**Figure 3.** (a) Simulation results of the $CO_2$ concentration distribution based on diffusion equations. (b) Potential-dependent current density on 4.7 nm Cu NPs with different spacings. (c) Faradaic selectivity of 4.7 nm Cu NPs as a function of the interparticle distance. Panels a−c reproduced with permission from ref 14. Copyright 2016 American Chemical Society. (d) Potential-dependent ethylene/methane FE ratio over $CuO_x$ NPs with different Cu loadings. Reproduced with permission from ref 15. Copyright 2017 Wiley.

selective electrocatalysts. Recurrent topics throughout our report are the need of having access to morphologically and chemically well-defined material systems to establish structure/chemical state/composition-reactivity correlations, and to able to study them in situ and under operando reaction conditions to gain mechanistic insight into $CO_2$RR.

## 2. FROM MOLECULAR CATALYSTS TO SINGLE-SITE HETEROGENEOUS CATALYSTS

Because of the intrinsically high metal atom efficiency, molecular catalysts usually show high turnover frequency (TOF) for many chemical reactions, including $CO_2$RR.[2,3] Cobalt porphyrins incorporated in covalent organic frameworks exhibited 90% Faradaic efficiency (FE) and TOF of 9400 $h^{-1}$ with an overpotential of −0.55 V for $CO_2$RR to CO.[2] Single site heterogeneous catalysts, with isolated metal atoms embedded in a nitrogen-doped carbon matrix, have been explored for $CO_2$RR.[4−6] Ju et al.[4] studied the $CO_2$RR performance of a family of single site, metal- and nitrogen-doped nanoporous carbons (Figure 1) containing active M−$N_x$ sites (M = Mn, Fe, Co, Ni, Cu). Fe−$N_x$ and Ni−$N_x$ single-site catalysts showed a unique reactivity and FE for reducing $CO_2$ to CO, comparable to the mass-based activity of state-of-the-art Au catalysts. Wang et al.[5] further reported that single-site Co catalysts exhibit a remarkable activity and selectivity toward $CO_2$RR if the Co−N coordination number decreases from 4 to 2 because of the facilitated activation of $CO_2$ to the $CO_2^{\bullet-}$intermediate over low-coordinated sites.

## 3. METAL CLUSTER AND NANOPARTICLE (NP) SIZE EFFECTS

Metal clusters and NPs have been explored for $CO_2$RR because of their high surface-to-volume-ratio and large content of low-coordinated surface sites. For example, $Au_{25}$ clusters experience a charge redistribution induced by a reversible $Au_{25}$−$CO_2$ interaction[7] that results in a 200−300 mV lower overpotential and a CO production rate 200−700 times higher as compared to 5 nm Au NPs and bulk Au. On the other hand, metal NPs usually show a size effect for $CO_2$RR.[8−13] Enhanced catalytic activity, unfortunately accompanied by a drastic increase in the selectivity for $H_2$ and CO in detriment of hydrocarbon production, was observed with decreasing Cu NP size (2−15 nm), Figure 2a.[8] Although size-dependent changes in the electronic structure of clusters are important (a few tens of atoms to about 100 atoms), for larger NPs as those in the previous example, size-dependent changes in surface atomic coordination are held responsible for the distinct catalytic reactivity. Thus, the increased population of low-coordinated surface sites on the smaller Cu NPs (Figure 2b) was linked to the increased activity and surging $H_2$ and CO production rates. Au NPs showed a similar size effect, but with a more drastic increase in activity with decreasing size,[9] along with a decrease in CO selectivity which was explained by the weaker binding of the COOH reaction intermediate in the presence of large H coverages on the small Au NPs (Figure 2c).[10] Interestingly, a simultaneous increase in current density and CO FE was observed for Pd NPs with decreasing size (Figure 2d).[11] The different behavior between Au and Pd NPs was attributed to the similar activity of the competitive HER on the terrace, edge and corner sites of the Pd NPs, instead of the more favored HER on the undercoordinated sites of the Au NPs.[10]

## 4. INTERPARTICLE DISTANCE/LOADING EFFECT

Apart from the nanoscale structure and composition, mesoscale phenomena such as interparticle reactant diffusion and readsorption of intermediates also play a key role in reactivity.[14] Cu NPs with narrow NP size distributions and uniform arrangements were used as model material system. For



DOI: 10.1021/acs.accounts.8b00360
Acc. Chem. Res. 2018, 51, 2906−2917

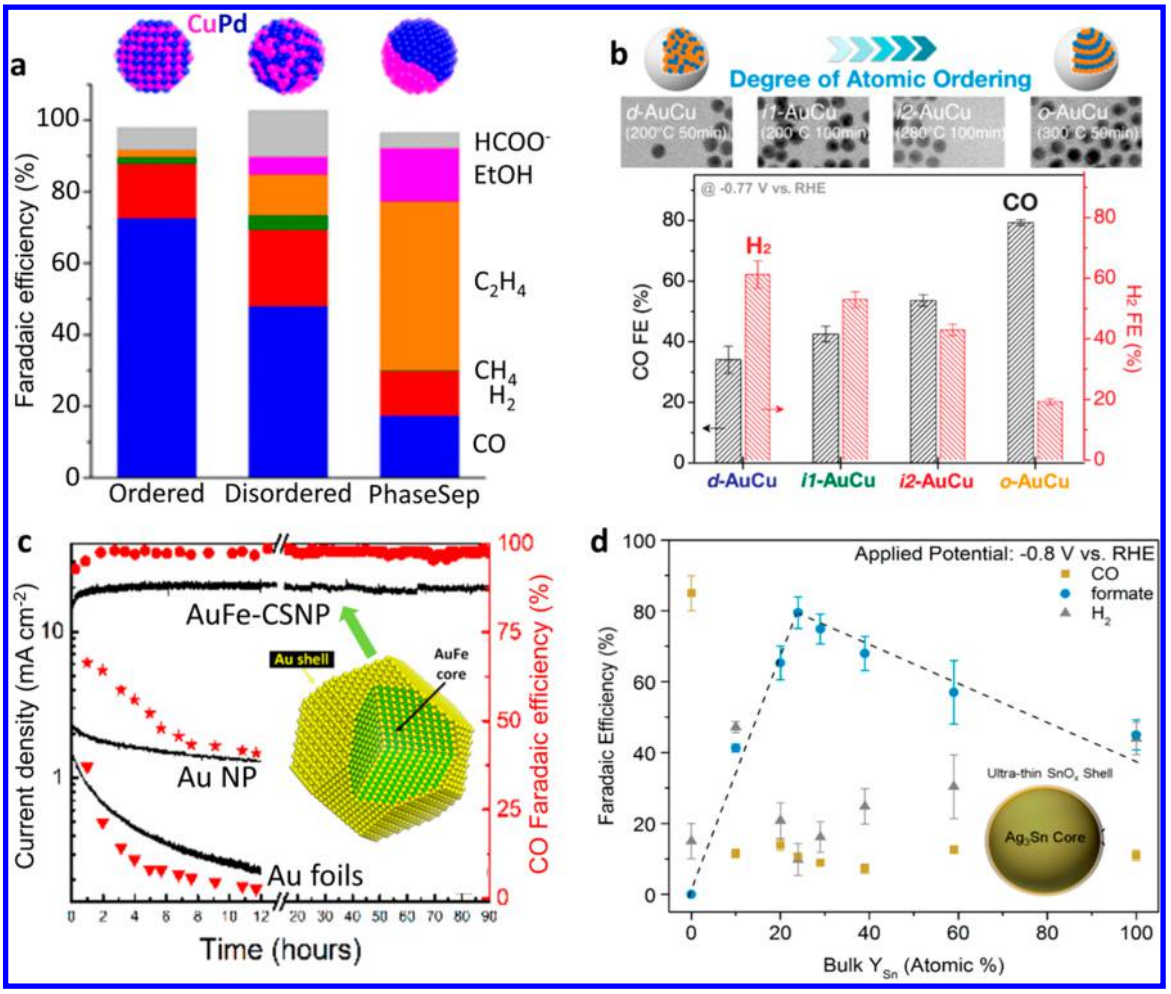


**Figure 4.** (a) Product distribution of CuPd NPs with different atomic arrangements. Reproduced with permission from ref 19. Copyright 2017 American Chemical Society. (b) CO and $H_2$ selectivities of AuCu NPs with different atomic ordering. Reproduced with permission from ref 20. Copyright 2017 American Chemical Society. (c) Stability of AuFe@Au core−shell NPs. Reproduced with permission from ref 22. Copyright 2017 American Chemical Society. (d) Correlations between FE of products and composition of AgSn core−shell NPs. Reproduced with permission from ref 23 Copyright 2017 American Chemical Society.

the same average NP size, a trend of increasing current density with decreasing interparticle (IP) distance was found. Furthermore, on samples with small IP spacing the diffusive transfer between neighboring NPs as well as the readsorption and subsequent reduction of the CO intermediate to hydrocarbons was favored, Figure 3a−c. However, the important role of changes in the local pH resulting from the distinct depletion of reactants and intermediates on samples with different spacings cannot be overlooked. Subsequently, Wang et al.[15] explored indirectly the IP distance effect on the selectivity of $CO_2$RR on $CuO_x$ NPs by changing the areal particle density, Figure 3d. They found that high areal particle density (small IP distance) improved ethylene production and attributed this to dynamically favored CO readsorption and reactive *CO dimerization at elevated local interfacial pH. The IP distance effect was also observed for the oxygen reduction reaction over Pt nanoclusters.[16] A distinct potential distribution in the electric double layer (EDL) between the nanoclusters was suggested to lower the adsorption strength of oxygenated species and hence improve the activity at small IP distances.[16] However, this effect cannot explain IP-distance dependent $CO_2$RR data since the smallest distances studied (~20 nm) are significantly larger than the ones deemed relevant for the EDL overlap in ref 16 (≤3 nm). The role of the Cu loading in the dynamic evolution from densely packed Cu NPs to cube-like particles was also observed by Kim et al.[17] and Manthiram et al.[18] during $CO_2$RR.

## 5. BIMETALLIC CATALYSTS

Bimetallic catalysts, with various compositions and atomic arrangements, might be used to tune the binding strength of intermediates, to enhance the reaction kinetics and change the reaction pathways for $CO_2$RR. The relatively low selectivity toward hydrocarbons and oxygenates on Cu NPs may be improved by designing bimetallic CuPd catalysts (Figure 4a).[19] Phase-separated CuPd catalyst were found to achieve high selectivity (>60%) for $C_2$, while ordered CuPd catalyst with an alternating Cu−Pd arrangement exhibited the highest selectivity for $C_1$ (>80%). Geometric/structural effects, as well as electronic effects induced after mixing Cu with Pd, appear to play an important role in determining the subsequent reaction pathway of the *CO intermediate. Similar geometric effects were also observed for AuCu NPs. In contrast to AuCu alloy NPs which were more active for HER, ordered AuCu NPs selectively converted $CO_2$ to CO with a FE of 80% (Figure 4b).[20] However, the negative potentials being used for


DOI: 10.1021/acs.accounts.8b00360
Acc. Chem. Res. 2018, 51, 2906−2917

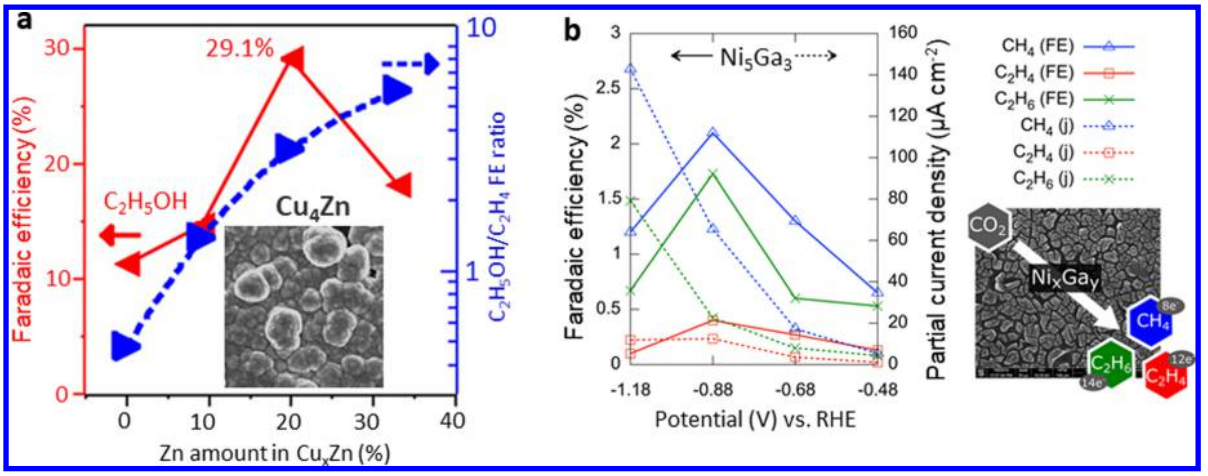


**Figure 5.** (a) Ethanol FE and ethanol to ethylene ratio as a function of the Zn content in $Cu_xZn$ films. The insert is an SEM image of a $Cu_4Zn$ film. Reproduced with permission from ref 25. Copyright 2016 American Chemical Society. (b) Potential-dependent hydrocarbon FE and partial current density for $Ni_5Ga_3$ films. An SEM image of a $Ni_xGa_y$ film is also shown. Reproduced with permission from ref 26. Copyright 2016 American Chemical Society.

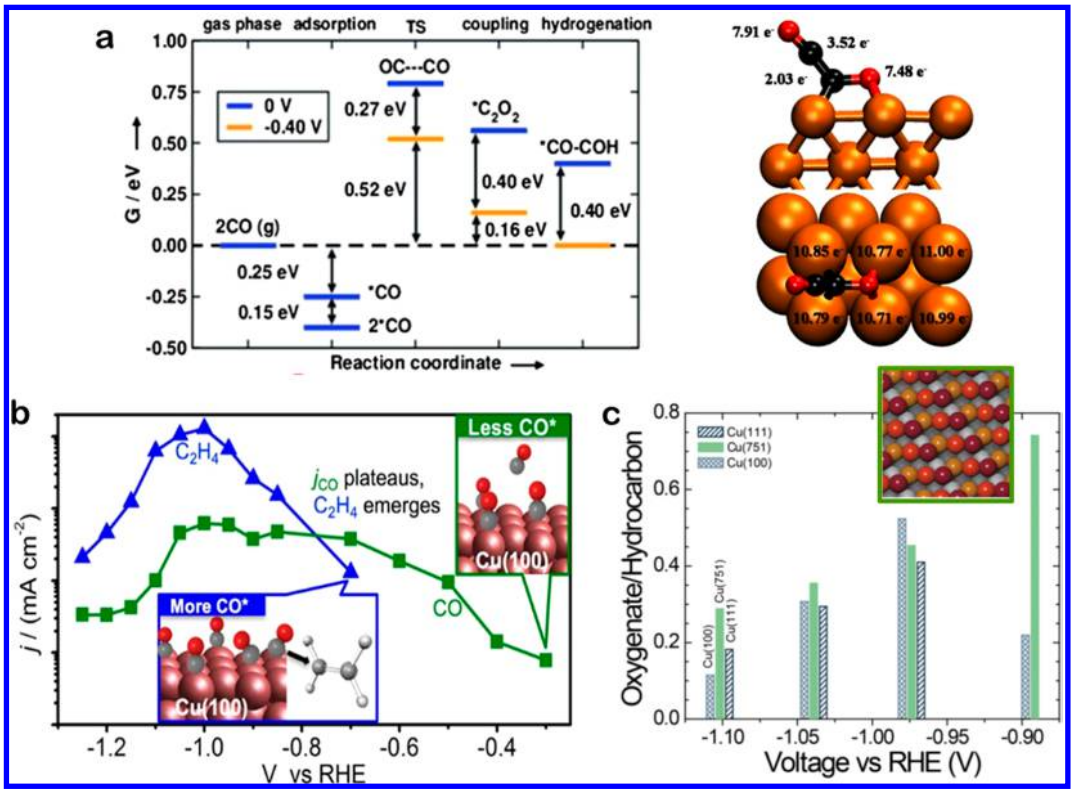


**Figure 6.** (a) Deconvolution of the first electron−proton transfer at 0 $V_{SHE}$ and −0.4 $V_{SHE}$ on Cu(100), and adsorption geometry and Bader charges of the dimer and the surface. C black, O red, Cu orange. Reproduced with permission from ref 31. Copyright 2013 Wiley. (b) Relationship between ethylene formation and CO evolution on Cu(100) during $CO_2$RR. Reproduced with permission from ref 32. Copyright 2017 American Chemical Society. (c) Oxygenate/hydrocarbon ratios as a function of potential for Cu(111), Cu(751), and Cu(100) and atomic model of the Cu(751) surface (inset). Reproduced with permission from ref 33. Copyright 2017 Proceedings of the National Academy of Science.

the $CO_2$RR process are expected to induce significant segregation in bimetallic NPs, such as the formation of an Au-rich surface.[21] Along these lines, core−shell AuFe@Au NPs with surface defects stabilized by subsurface Fe were found to exclusively produce CO with a 100-fold increase in mass activity compared to Au NPs, Figure 4c.[22] AgSn@$SnO_x$ core−shell NPs showed a volcano-like relationship between formate production and Sn concentration, attributed to the compromise of favorable stabilization of OCHO* by lattice expansion and the electron conductivity loss due to the increased thickness of the $SnO_x$ shell (Figure 4d).[23] A greater alcohol to ethylene ratio was achieved by including sulfur atoms in Cu NPs. According to density functional theory (DFT) calculations, the resulting Cu vacancies in the NP shell were responsible for the higher alcohol production.[24]

In addition to NPs, bimetallic films were also used for $CO_2$RR. By varying the amount of Zn in $Cu_xZn$ film catalysts, the selectivity for ethanol versus ethylene production could be



DOI: 10.1021/acs.accounts.8b00360
Acc. Chem. Res. 2018, 51, 2906−2917

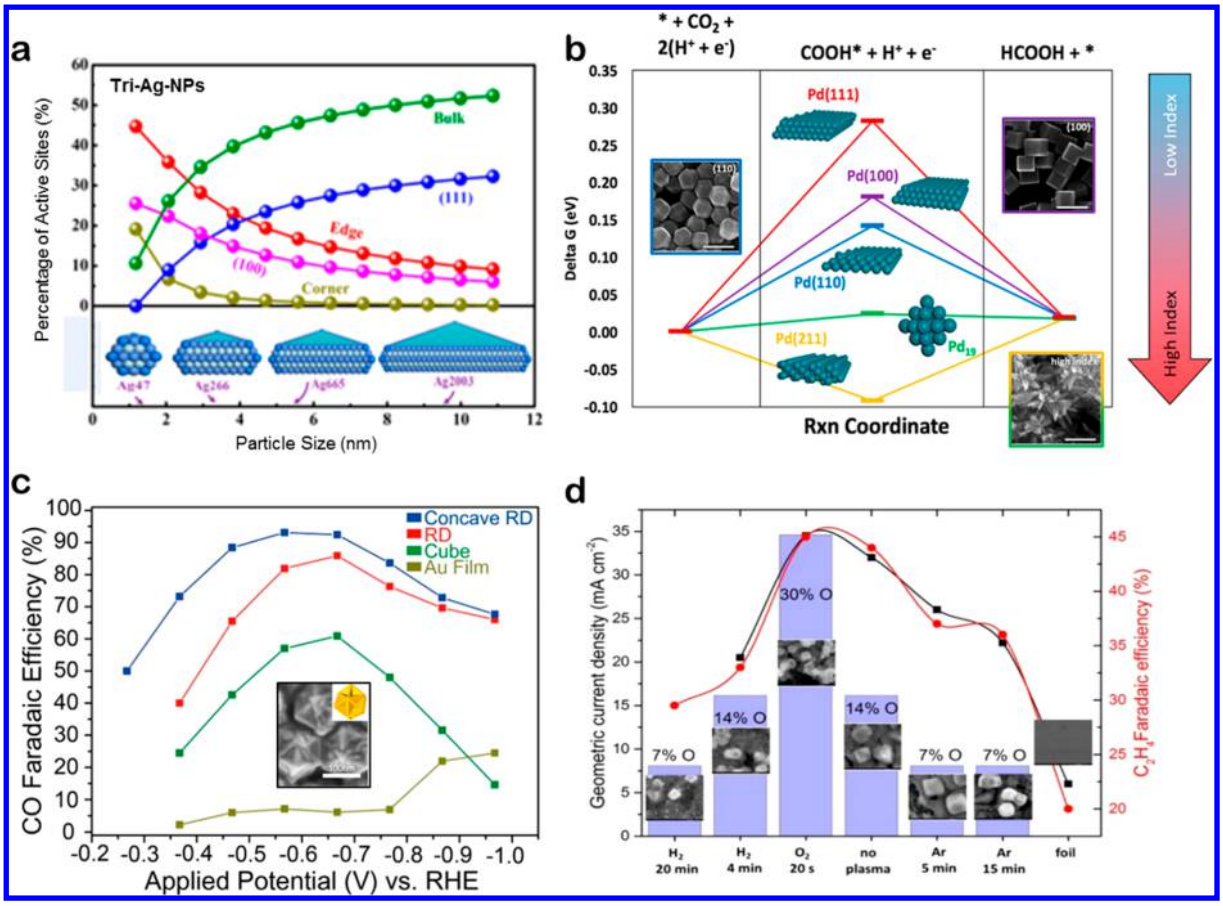


**Figure 7.** (a) Active adsorption site density on triangular Ag nanoplates as a function of particle size. Reproduced with permission from ref 35. Copyright 2017 American Chemical Society. (b) Free energy diagrams for $CO_2RR$ to formic acid, and free energies of CHOO* and CO* intermediates on Pd single crystal surfaces of different orientations and a $Pd_{19}$ cluster. The reaction energy barrier is significantly decreased as the index increases. Reproduced with permission from ref 34. Copyright 2016 American Chemical Society. (c) CO FE of an Au film and shaped Au NPs (cubic, rhombic dodecahedron (RD) and concave RD) at −1.0 $V_{RHE}$. Reproduced with permission from ref 36. Copyright 2015 American Chemical Society. (d) Current density and ethylene FE at −1.0 $V_{RHE}$ for different plasma-treated Cu nanocubes and an electropolished Cu foil. Reproduced with permission from ref 38. Copyright 2017 American Chemical Society.

tuned, Figure 5a. It was discussed that CO spillover from Zn to adjacent Cu sites increased the population of free CO, which participates in the formation of ethanol by inserting itself into the bond between the Cu surface and $*CH_2$.[25] $Ni_xGa_y$ (Figure 5b) constitutes an example of hydrocarbon production on non-Cu materials.[26] The introduction of Ga into the Ni films weakened the Ni-CO interaction, resulting in a comparable CO binding strength as CO-Cu. The formation of more reduced products beyond CO was recently described to depend on an optimum binding of both, CO and H.[27] This strategy was applied to Pd-modified-Au foils,[28] which also produced hydrocarbons (<5% FE).

## 6. FACET EFFECT: FROM SINGLE CRYSTAL ELECTRODES TO SHAPED NPS

Over the past decades, single crystal studies have provided in depth insight on the influence of the surface structure and order in electrocatalytic processes of technical interest.[1] As aforementioned, Cu is unique at converting $CO_2$ into hydrocarbons and alcohols, mainly because of its moderate CO binding and the stabilization of certain intermediates.[29] Moreover, the product selectivity is highly dependent on the crystalline orientation: Cu(111) yields mainly methane, while Cu(100) favors ethylene, and Cu(110) promotes the production of ethanol, acetate, and acetaldehyde.[1,30] Theoretical studies have shed light into the reaction mechanisms and intermediates responsible for the different selectivity on (111) and (100) surfaces,[31] showing that the atomic configuration of the Cu(100) surface is the most favorable toward the pathway that yields ethylene. This mechanism was argued to take place via CO dimerization, Figure 6a. In this sense, high surface coverage of adsorbed CO* was found essential for the selective formation of ethylene (Figure 6b).[32] Moreover, Cu(751) surfaces show higher selectivity for $C_{2+}$ products at lower overpotentials than lower indexed surfaces, Figure 6c.[33] However, the role played by the distinct facets in $CO_2RR$ is not fully understood, and further studies using model surfaces are still needed to understand the combined effect of surface structure and other parameters, such as oxygen content.

Nanoparticles synthesized with a particular morphology generally have a well-defined surface structure. Therefore, tailoring the shape of the NPs can lead to materials with superior activity and selectivity. Facet effects on metals like Pd,[34] Ag[35] and Au[36] have been explored for $CO_2RR$, showing the importance of the structure for CO and formate production. For instance, Ag(100) facets lead to an ultralow overpotential for $CO_2$ reduction to CO on triangular Ag nanoplates (Figure 7a), while enhanced activity and selectivity


DOI: 10.1021/acs.accounts.8b00360
Acc. Chem. Res. 2018, 51, 2906−2917

for either formate or CO was found for Pd and Au NPs, respectively (Figure 7b and c). Regarding Cu, cubic-shaped NPs composed of (100) facets were found to display increased ethylene selectivity while suppressing methane production.[37,38] The presence of small well-ordered (100) domains, combined with numerous steps and edges could be responsible for this selectivity trend as proposed for stepped surfaces.[1] However, other facts might also determine the selectivity toward the formation of $C_{2+}$ products. Gao et al.[38] recently demonstrated the combined effect of morphology, defect density and oxygen content on the activity and selectivity of Cu nanocubes modified by plasma treatments. The presence and stabilization of subsurface oxygen and $Cu^+$ species under reaction conditions were key parameters to favor $C_{2+}$ product selectivity (Figure 7d).

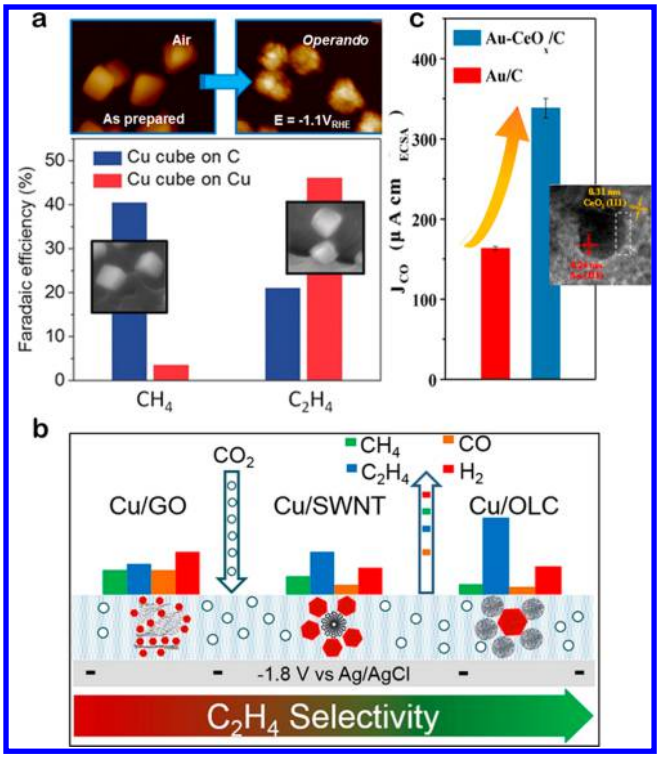


**Figure 8.** (a) Electrochemical atomic force microscopy (EC-AFM) images of Cu-cubes on highly oriented pyrolytic graphite (HOPG) before and during $CO_2$RR at −1.1 $V_{RHE}$, and effect of the support (C vs Cu) in methane and ethylene FEs. Reproduced with permission from ref 39. Copyright 2018 Wiley. (b) Structure effect of the C support on $CO_2$RR over Cu NPs: single wall carbon nanotubes (SWNT), reduced graphene oxide (RGO) and onion-like carbon (OLC). Reproduced with permission from ref 40. Copyright 2017 Elsevier. (c) Enhanced CO production on Au−$CeO_x$ catalysts. Reproduced with permission from ref 41. Copyright 2017 American Chemical Society.

## 7. STABILITY AND SUPPORT EFFECT

Dynamic changes in the morphology of shaped electrocatalysts in the course of the $CO_2$RR cannot be neglected, since they might have ascribed concomitant changes in the resulting activity and selectivity. For example, surface roughening, defect and pore formation, and the disappearance of well-defined (100) facets on Cu nanocubes deposited on carbon, together with a reduction of $CuO_x$ species, were found to be responsible of a significantly lower selectivity toward ethylene and ethanol in favor of methane.[39] The effect of the support was also explored, showing an enhanced morphological durability and greater stability of $Cu^+$ species under $CO_2$RR when a Cu foil was used as support instead of carbon. Furthermore, the Cu cubes on Cu-foil[38] displayed a lower overpotential and higher FE for $C_{2+}$ products than those on C (Figure 8a).[39] Carbon supports with different morphologies have also been explored for Cu NPs to increase the CO surface concentration and thus facilitate its dimerization and ethylene production (Figure 8b).[40] Strong interactions at metal/metal-oxide interfaces were found to be responsible for higher reactivity and stability. For instance, Au NPs supported on $CeO_x$ showed higher CO FE than those supported on C, which was ascribed to an enhanced $CO_2$ activation at the Au−$CeO_x$ interface (Figure 8c).[41]

## 8. ROUGHNESS AND DEFECTS

Nanostructured materials show better catalytic activity and selectivity than flat surfaces. The presence of low coordinated sites, such as steps, edges and defects,[42] grain boundaries,[43] or certain periodic spacing between the facets at the electrode surface,[1] are thought to be responsible for the enhanced reactivity. The in situ electrochemical reduction of metal oxides offers a way to prepare roughened and highly defective structures that exhibit higher current densities compared to flat surfaces due to their larger electrochemically active surface areas.[44] However, the selectivity for $CO_2$RR of these systems is also drastically modified. Roughened and highly defective Cu surfaces display preferential selectivity toward multicarbon products and oxygenates.[38,42,45−47]

On the other hand, high CO yield at lower overpotentials has been found for highly porous Au, Ag, and Zn catalysts. For example, the improved catalysis in oxide-derived (OD) Au electrodes, which showed >96% FE for CO at −0.35 V vs RHE over the course of 8 h electrolysis, has been ascribed to a better stabilization of the $CO_2^{\bullet-}$ intermediate (Figure 9a).[48] In the same way, $O_2$-plasma pretreated highly defective nanostructured Ag catalysts showed CO FE above 90% at −0.6 V vs RHE, a notable enhancement over flat Ag foils, which reduces $CO_2$ at overpotentials below −0.9 V vs RHE.[49] The operando X-ray absorption fine-structure spectroscopy (XAFS) and quasi in situ X-rayphotoelectron spectroscopy (XPS) characterization of these samples revealed that the surface $AgO_x$ species are reduced within the first 3 min of the reaction, and that subsurface oxygen or $AgO_x$ is not detected either in the bulk of the foil after 35 min, ruling out the role of $AgO_x$ or O in their improved reactivity, Figure 9b. Instead, DFT calculations indicated that defects created by the plasma treatment lead to locally enhanced negative electric fields which resulted in a decrease in the overpotential needed to produce CO.

## 9. OXIDATION STATE EFFECT

Oxide-derived Cu catalysts have been proven to be very selective for the formation of $C_{2+}$ products.[50] Structural factors, such as roughness effects, defects, and grain boundaries left behind by the oxygen pretreatment have been initially deemed responsible for the former unusual reactivity, although more recently the presence of $Cu^+$ and residual subsurface oxygen have been suggested to influence the formation of ethylene and


DOI: 10.1021/acs.accounts.8b00360
Acc. Chem. Res. 2018, 51, 2906−2917

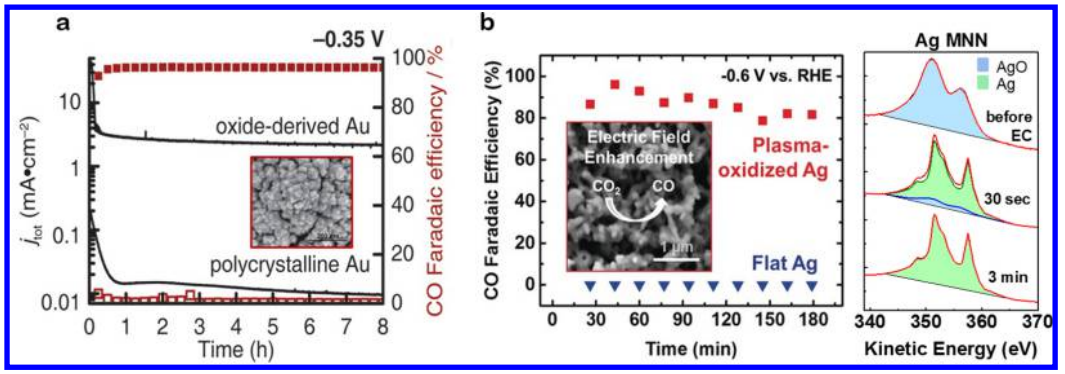


**Figure 9.** Comparison of $CO_2R$ selectivity of planar polycrystalline M (M = Au, Ag) with that of (a) OD-Au NPs and (b) $O_2$ plasma-treated Ag foil. The Ag MNN Auger region of the former sample before and after short $CO_2RR$ reaction times is shown. Panel a reproduced with permission from ref 48. Copyright 2012 American Chemical Society. Panel b reproduced with permission from ref 49. Copyright 2017 Wiley.

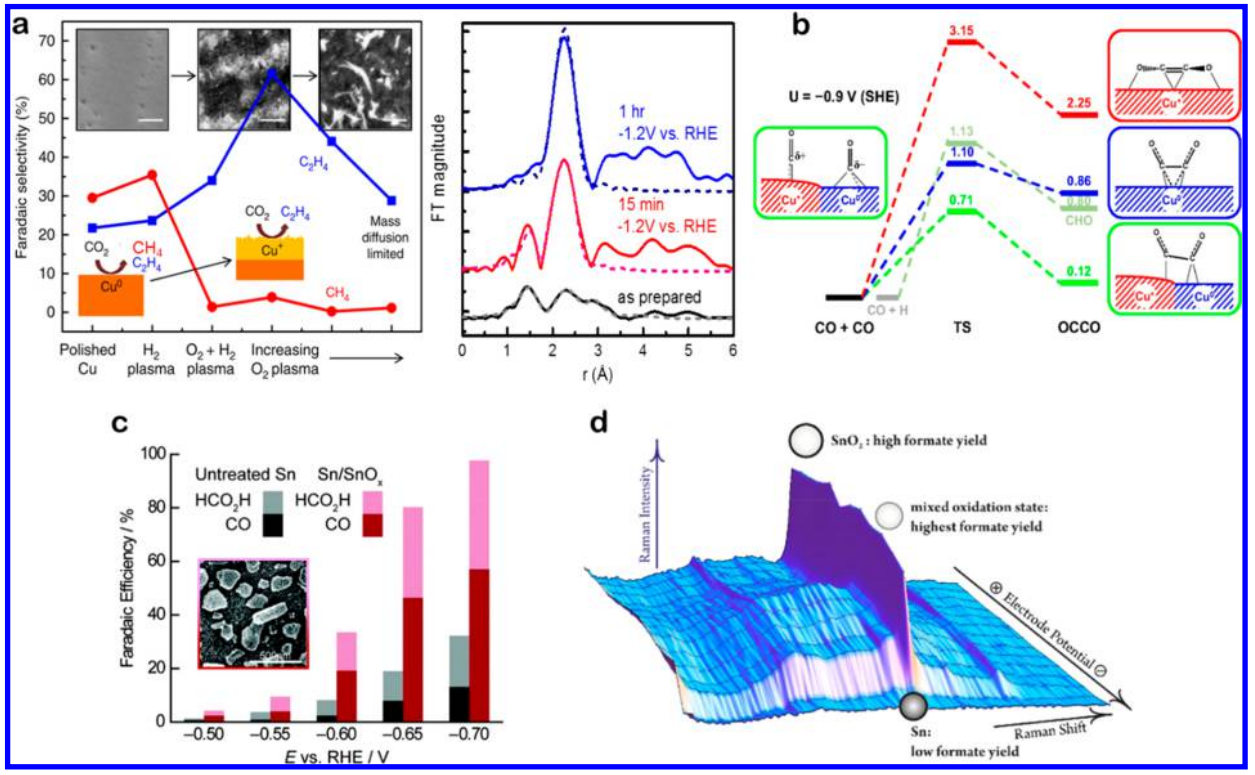


**Figure 10.** (a) Hydrocarbon selectivity of plasma-treated Cu foils and EXAFS spectra with fits acquired under operando $CO_2RR$ conditions. Reproduced with permission from ref 45. Copyright 2016 Nature Publishing Group. (b) Free energy profiles of CO dimerization on a fully oxidized (red), metallic (blue), and Cu metal in oxidized (green) matrixes. Reproduced with permission from ref 57. Copyright 2017 Proceedings of the National Academy of Science. (c) HCOOH and CO FEs for Sn foil (gray and black) and in situ-deposited $Sn/SnO_x$ thin film (pink and red) electrodes. Inset shows a SEM image of the in situ-deposited $Sn/SnO_x$ thin film. Reproduced with permission from ref 60. Copyright 2012 American Chemical Society. (d) Potential-dependent Raman spectra of a $SnO_2$ surface under operando $CO_2RR$ conditions. Reproduced with permission from ref 61. Copyright 2015 American Chemical Society.

alcohols.[51,52] Still, significant reduction of the OD Cu catalyst to metallic state is bound to occur during $CO_2$ electroreduction.[53] In fact, a number of studies have reported metallic Cu as the only stable and active species during $CO_2RR$.[29,58] However, special sites can be created in the Cu structures to stabilize the $Cu^+$ species or subsurface oxygen. For instance, the inclusion of boron as a modifier element can change the electronic structure of Cu and stabilize $Cu^{\delta+}$. The latter was theoretically and experimentally linked to a higher selectivity toward $C_2$ products from $CO_2RR$.[54]

The presence of $Cu^+$ species and subsurface oxygen during $CO_2RR$ was experimentally demonstrated via operando XAFS (Figure 10a).[45] Although the roughness of these plasma-treated OD-catalysts played a role in contributing to their increased activity, their outstanding ethylene selectivity (up to 60%) was found to correlate with the presence of $Cu^+$ and subsurface oxygen. The role of $CuO_x$ species and oxygen in Cu had been also previously discussed by others,[55] but only based on ex situ measurements,[56] which had been questioned due to the facile oxidation of Cu upon air exposure for the characterization. A subsequent theoretical study described a synergistic effect between neighboring $Cu^+$ and $Cu^0$ in Cu surfaces leading to improved kinetics and thermodynamics of both $CO_2$ activation and CO dimerization, while hindering the


DOI: 10.1021/acs.accounts.8b00360
Acc. Chem. Res. 2018, 51, 2906−2917

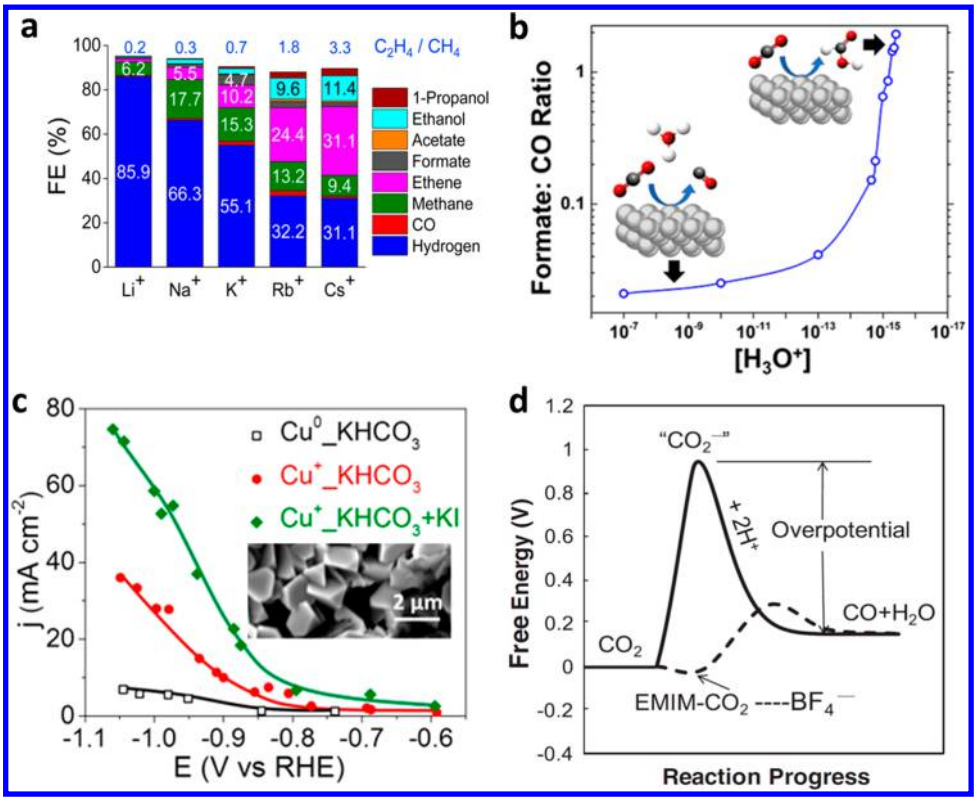


**Figure 11.** (a) FEs for $CO_2$RR products over Cu at −1.0 $V_{RHE}$ in $CO_2$-saturated 0.1 M $MHCO_3$ (M = $Li^+$, $Na^+$, $K^+$, $Rb^+$, $Cs^+$) electrolyte. Reproduced with permission from ref 62. Copyright 2016 American Chemical Society. (b) Formate to CO FE ratio as a function of hydronium concentration on Ag. Reproduced with permission from ref 70. Copyright 2018 American Chemical Society. (c) Halide effect on the reactivity and surface reconstruction (inset) of $O_2$-plasma pretreated Cu foils. Reproduced with permission from ref 71. Copyright 2017 American Chemical Society. (d) Free energy of $CO_2$RR to CO on Ag with and without EMIM-$BF_4$. Reproduced with permission from ref 75. Copyright 2011 Science Publishing Group.

$C_1$ pathways (Figure 10b).[57] Despite these promising results, the catalytic role of $Cu^+$ and subsurface oxygen is a current topic of strong controversy.[58]

The effect of the metal oxidation state and the presence of subsurface oxygen is not only important for Cu. $SnO_x$ is essential for $CO_2$RR catalysis on Sn electrodes. DFT calculations point out that oxygen vacancies on the SnO surface are decisive for the selective reduction of $CO_2$ to formate.[59] Moreover, $SnO_x$ appears to provide chemical functionality that stabilizes the $CO_2^{\bullet-}$ intermediate, mediating the direct electron transfer that yields CO and HCOOH (Figure 10c).[60] Furthermore, on the basis of operando Raman spectroscopy, a decrease in the formate FE was assigned to the reduction of $SnO_x$ to metallic Sn (Figure 10d).[61] These results may open new perspectives in the preparation of metal/metal oxide composites with superior activity and selectivity.

## 10. ELECTROLYTE EFFECT

$CO_2$RR performance is generally measured in aqueous electrolytes, typically potassium bicarbonate solutions. Alkali metal cations have been reported to facilitate $CO_2$ adsorption and stabilize reaction intermediates.[62] On Cu electrodes, increasing the cation size leads to a decrease in FEs of $H_2$ and $C_1$, as well as an increase in $C_{2+}$ (Figure 11a).[62−64] This selectivity change could be explained by the preferential hydrolysis of the cations, lowing the local pH near the electrode, leading to higher local $CO_2$ concentration.[62] Bicarbonate is considered to contribute to the enhanced $CO_2$RR activity by increasing the effective $CO_2$ concentration near the electrode surface.[65−67] In addition, the bicarbonate solution can also suppress the increase of the local pH near the electrode surface, which significantly affects the reaction pathways for the production of methane and ethylene on Cu.[68] $CO_2$RR conducted in highly concentrated (10 M) KOH (high pH) over a Cu gas diffusion electrode revealed that the onset of ethylene evolution (−0.165 V vs RHE) occurs almost simultaneously with the CO production.[69] Similarly, the major product on Ag switched from CO at pH 7 to formate at pH > 15 (Figure 11b).[70]

Since the $CO_2$RR performance is very sensitive to the composition and nature of the electrolyte, a number of studies exist trying to improve $C_{2+}$ production via electrolyte design.[62,63,71,72] For example, by adding halide ions into the bicarbonate electrolyte,[71] the $CO_2$RR activity could be significantly increased without sacrificing the intrinsically high $C_{2+}$ selectivity of plasma-oxidized Cu catalysts (Figure 11c). Halide ions, such as $I^-$, can also induce significant nanostructuring of the oxidized Cu surface, even at open circuit potential. The stabilization of $Cu^+$ species made the halide effect on oxidized Cu different from that on metallic Cu, where an increased methane production is observed in contrast to ethylene production over $CuO_x$.[72]

In aqueous electrolytes, the reaction rate of $CO_2$RR is usually mass transport-limited due to the low $CO_2$ solubility in water (33 mM at 25 °C, 1 atm). To overcome this disadvantage, high $CO_2$ pressure[73] and supercritical $CO_2$[74] have been explored to increase the $CO_2$ concentration in aqueous electrolytes. Additionally, organic solvents, such as


DOI: 10.1021/acs.accounts.8b00360
Acc. Chem. Res. 2018, 51, 2906−2917

acetonitrile, methanol, and *N*,*N*-dimethylformamide, are also used because of their improved $CO_2$ solubility compared to water. Ionic liquids can also be employed as cocatalysts, either as electrolytes dissolved in a solvent, or as combined solvent/electrolyte. Rosen et al.[75] reported an electrocatalytic system with 1-ethyl-3-methylimidazolium tetrafluoroborate (EMIM-$BF_4$) as an electrolyte in water which was able to reduce $CO_2$ to CO at overpotentials below 0.2 V with >96% FE. The ionic liquid lowered the energy of the $CO_2^{\bullet-}$ intermediate and the initial reduction barrier (Figure 11d).

## 11. CONCLUSION

In summary, structure- and electrolyte-reactivity relationships in $CO_2$RR have been exemplified over a number of molecular, nanostructured, and single crystal catalysts. Although the dynamic changes of the morphology, atomic arrangement, coordination number, and oxidation state of the catalysts under reaction conditions can already be monitored by advanced operando microscopy and spectroscopic techniques, improved surface sensitivity of some of this methods (e.g., XAFS) is still needed when surface-modified bulk systems are studied. Furthermore, challenges still exist when trying to conduct truly surface-sensitivity measurements (e.g., XPS) not only quasi in situ but also in a flow-cell configuration under potential control.

Moreover, the greater complexity of real catalysts compared to model single crystals further motivates researchers to try to synthesize well-defined nanoscale systems, where one could obtain in depth understanding of the different parameters affecting $CO_2$RR by isolating, when possible, different contributions, as for example the role of the NP size, shape, structure, oxidation state, composition, interparticle distance, etc. Adding to this challenging task is the need of understanding the complexity of electrified solid/liquid and solid/liquid/gas interfaces. For instance, the adsorption of anions and cations on the electrode surface is usually different in the presence of applied potentials, and the adsorbed species also interact with $CO_2$ and reaction intermediates differently when electric fields are considered.

In the coming years, being able to gain in depth atomistic/molecular insight into the complexity of electrode/electrolyte interfaces, including their interaction under different environmental conditions will be key for understanding $CO_2$RR mechanisms and further designing more active and selective catalysts.

## AUTHOR INFORMATION


### Corresponding Author

*E-mail: roldan@fhi-berlin.mpg.de.

### ORCID

Rosa M. Arán-Ais: 0000-0001-9892-1980
Dunfeng Gao: 0000-0002-2472-7349
Beatriz Roldan Cuenya: 0000-0002-8025-307X

### Author Contributions

§R.M.A.A. and D.G. contributed equally to this work.


### Notes

The authors declare no competing financial interest.

### Biographies

**Rosa M. Arán-Ais** obtained her B.Sc. in Chemistry from the University of Alicante (Spain) in 2010 and her Ph.D. at the same University in 2016. She is now a postdoctoral researcher in the Department of Physics at the Ruhr-University Bochum, Germany. Her research interests include gaining fundamental insight on electrocatalytic processes based on single crystal work, as well as the synthesis, characterization, and electrocatalysis of size- and shape-controlled metal NPs.

**Dunfeng Gao** received his B.Sc. in Materials Chemistry from the China University of Petroleum in 2009 and Ph.D. in Physical Chemistry from the Dalian Institute of Chemical Physics, Chinese Academy of Sciences in 2015. Currently, he is a postdoctoral researcher in the Department of Interface Science at the Fritz-Haber Institute of the Max Planck Society, Germany. His research focuses on developing highly efficient nanostructured catalysts for $CO_2$RR.

**Beatriz Roldán Cuenya** completed her B.S. in Physics from the University of Oviedo, Spain in 1998. She obtained her Ph.D. from the Department of Physics of the University of Duisburg-Essen (Germany) in 2001. She then became a postdoctoral scholar in the Department of Chemical Engineering at the University of California Santa Barbara (2001−2003). In 2004, she joined the Department of Physics at the University of Central Florida (UCF) as Assistant Professor where she moved through the ranks to become a full professor in 2012. In 2013, she became a chair professor of Solid State Physics in the Department of Physics, Ruhr-University Bochum (2013−2017). Currently, she is the director of the Department of Interface Science at the Fritz-Haber Institute of the Max Planck Society (Berlin, Germany). Her research program explores physical and chemical properties of nanostructures, with emphasis on advancements in nanocatalysis based on operando microscopic and spectroscopic characterization.

## ACKNOWLEDGMENTS

This work was supported by the European Research Council under Grant ERC-OPERANDOCAT (ERC-725915) and the German Federal Ministry of Education and Research (BMBF) under Grants 03SF0523C-"CO2EKAT" and 033RCOO4D-"e-Ethylene".

## REFERENCES


(1) Hori, Y. Electrochemical $CO_2$ Reduction on Metal Electrodes. *Modern Aspects of Electrochemistry* **2008**, *42*, 89−189.

(2) Lin, S.; Diercks, C. S.; Zhang, Y.-B.; Kornienko, N.; Nichols, E. M.; Zhao, Y.; Paris, A. R.; Kim, D.; Yang, P.; Yaghi, O. M.; Chang, C. Covalent Organic Frameworks Comprising Cobalt Porphyrins for Catalytic $CO_2$ Reduction in Water. *Science* **2015**, *349*, 1208−1213.

(3) Göttle, A. J.; Koper, M. T. M. Determinant Role of Electrogenerated Reactive Nucleophilic Species on Selectivity during Reduction of $CO_2$ Catalyzed by Metalloporphyrins. *J. Am. Chem. Soc.* **2018**, *140*, 4826−4834.

(4) Ju, W.; Bagger, A.; Hao, G. P.; Varela, A. S.; Sinev, I.; Bon, V.; Roldan Cuenya, B.; Kaskel, S.; Rossmeisl, J.; Strasser, P. Understanding Activity and Selectivity of Metal-Nitrogen-Doped Carbon Catalysts for Electrochemical Reduction of $CO_2$. *Nat. Commun.* **2017**, *8*, 944.

(5) Wang, X.; Chen, Z.; Zhao, X.; Yao, T.; Chen, W.; You, R.; Zhao, C.; Wu, G.; Wang, J.; Huang, W.; Yang, J.; Hong, X.; Wei, S.; Wu, Y.; Li, Y. Regulation of Coordination Number over Single Co Sites: Triggering the Efficient Electroreduction of $CO_2$. *Angew. Chem., Int. Ed.* **2018**, *57*, 1944−1948.

(6) Huan, T. N.; Ranjbar, N.; Rousse, G.; Sougrati, M.; Zitolo, A.; Mougel, V.; Jaouen, F.; Fontecave, M. Electrochemical Reduction of $CO_2$ Catalyzed by Fe-N-C Materials: A Structure-Selectivity Study. *ACS Catal.* **2017**, *7*, 1520−1525.

(7) Kauffman, D. R.; Alfonso, D.; Matranga, C.; Qian, H.; Jin, R. Experimental and Computational Investigation of $Au_{25}$ Clusters and




DOI: 10.1021/acs.accounts.8b00360
*Acc. Chem. Res.* 2018, 51, 2906−2917

$CO_2$: A Unique Interaction and Enhanced Electrocatalytic Activity. *J. Am. Chem. Soc.* **2012**, *134*, 10237−10243.
(8) Reske, R.; Mistry, H.; Behafarid, F.; Roldan Cuenya, B.; Strasser, P. Particle Size Effects in the Catalytic Electroreduction of $CO_2$ on Cu Nanoparticles. *J. Am. Chem. Soc.* **2014**, *136*, 6978−6986.
(9) Zhu, W.; Michalsky, R.; Metin, Ö.; Lv, H.; Guo, S.; Wright, C.; Sun, X.; Peterson, A.; Sun, S. Monodisperse Au Nanoparticles for Selective Electrocatalytic Reduction of $CO_2$ to CO. *J. Am. Chem. Soc.* **2013**, *135*, 16833−16836.
(10) Mistry, H.; Reske, R.; Zeng, Z.; Zhao, Z. J.; Greeley, J.; Strasser, P.; Roldan Cuenya, B. Exceptional Size-Dependent Activity Enhancement in the Electroreduction of $CO_2$ over Au Nanoparticles. *J. Am. Chem. Soc.* **2014**, *136*, 16473−16476.
(11) Gao, D.; Zhou, H.; Wang, J.; Miao, S.; Yang, F.; Wang, G.; Wang, J.; Bao, X. Size-Dependent Electrocatalytic Reduction of $CO_2$ over Pd Nanoparticles. *J. Am. Chem. Soc.* **2015**, *137*, 4288−4291.
(12) Kim, C.; Jeon, H. S.; Eom, T.; Jee, M. S.; Kim, H.; Friend, C. M.; Min, B. K.; Hwang, Y. J. Achieving Selective and Efficient Electrocatalytic Activity for $CO_2$ Reduction Using Immobilized Silver Nanoparticles. *J. Am. Chem. Soc.* **2015**, *137*, 13844−13850.
(13) Zhang, S.; Kang, P.; Meyer, T. J. Nanostructured Tin Catalysts for Selective Electrochemical Reduction of $CO_2$ to Formate. *J. Am. Chem. Soc.* **2014**, *136*, 1734−1737.
(14) Mistry, H.; Behafarid, F.; Reske, R.; Varela, A. S.; Strasser, P.; Roldan Cuenya, B. Tuning Catalytic Selectivity at the Mesoscale via Interparticle Interactions. *ACS Catal.* **2016**, *6*, 1075−1080.
(15) Wang, X.; Varela, A. S.; Bergmann, A.; Kühl, S.; Strasser, P. Catalyst Particle Density Controls Hydrocarbon Product Selectivity in $CO_2$ Electroreduction on $CuO_x$. *ChemSusChem* **2017**, *10*, 4642−4649.
(16) Nesselberger, M.; Roefzaad, M.; Fayçal Hamou, R.; Ulrich Biedermann, P.; Schweinberger, F. F.; Kunz, S.; Schloegl, K.; Wiberg, G. K. H.; Ashton, S.; Heiz, U.; Mayrhofer, K. J. J.; Arenz, M. The Effect of Particle Proximity on the Oxygen Reduction Rate of Size-Selected Platinum Clusters. *Nat. Mater.* **2013**, *12*, 919−924.
(17) Kim, D.; Kley, C. S.; Li, Y.; Yang, P. Copper Nanoparticle Ensembles for Selective Electroreduction of $CO_2$ to $C_2$−$C_3$ Products. *Proc. Natl. Acad. Sci. U. S. A.* **2017**, *114*, 10560−10565.
(18) Manthiram, K.; Beberwyck, B. J.; Alivisatos, A. P. Enhanced Electrochemical Methanation of $CO_2$ with a Dispersible Nanoscale Copper Catalyst. *J. Am. Chem. Soc.* **2014**, *136*, 13319−13325.
(19) Ma, S.; Sadakiyo, M.; Heima, M.; Luo, R.; Haasch, R. T.; Gold, J. I.; Yamauchi, M.; Kenis, P. J. A. Electroreduction of $CO_2$ to Hydrocarbons Using Bimetallic Cu-Pd Catalysts with Different Mixing Patterns. *J. Am. Chem. Soc.* **2017**, *139*, 47−50.
(20) Kim, D.; Xie, C.; Becknell, N.; Yu, Y.; Karamad, M.; Chan, K.; Crumlin, E. J.; Nørskov, J. K.; Yang, P. Electrochemical Activation of $CO_2$ through Atomic Ordering Transformations of AuCu Nanoparticles. *J. Am. Chem. Soc.* **2017**, *139*, 8329−8336.
(21) Mistry, H.; Reske, R.; Strasser, P.; Roldan Cuenya, B. Size-Dependent Reactivity of Gold-Copper Bimetallic Nanoparticles during $CO_2$ Electroreduction. *Catal. Today* **2017**, *288*, 30−36.
(22) Sun, K.; Cheng, T.; Wu, L.; Hu, Y.; Zhou, J.; Maclennan, A.; Jiang, Z.; Gao, Y.; Goddard, W. A.; Wang, Z. Ultrahigh Mass Activity for $CO_2$ Reduction Enabled by Gold−Iron Core−Shell Nanoparticles. *J. Am. Chem. Soc.* **2017**, *139*, 15608−15611.
(23) Luc, W.; Collins, C.; Wang, S.; Xin, H.; He, K.; Kang, Y.; Jiao, F. Ag−Sn Bimetallic Catalyst with a Core−Shell Structure for $CO_2$ Reduction. *J. Am. Chem. Soc.* **2017**, *139*, 1885−1893.
(24) Zhuang, T.-T.; Liang, Z.-Q.; Seifitokaldani, A.; Li, Y.; De Luna, P.; Burdyny, T.; Che, F.; Meng, F.; Min, Y.; Quintero-Bermudez, R.; Dinh, C. T.; Pang, Y.; Zhong, M.; Zhang, B.; Li, J.; Chen, P.; Zheng, X.; Liang, H.; Ge, W.; Ye, B.; Sinton, D.; Yu, S.; Sargent, E. H. Steering Post-C−C Coupling Selectivity Enables High Efficiency Electroreduction of $CO_2$ to Multi-Carbon Alcohols. *Nat. Catal.* **2018**, *1*, 421−428.
(25) Ren, D.; Ang, B. S. H.; Yeo, B. S. Tuning the Selectivity of $CO_2$ Electroreduction toward Ethanol on Oxide-Derived $Cu_xZn$ Catalysts. *ACS Catal.* **2016**, *6*, 8239−8247.
(26) Torelli, D. A.; Francis, S. A.; Crompton, J. C.; Javier, A.; Thompson, J. R.; Brunschwig, B. S.; Soriaga, M. P.; Lewis, N. S. Nickel-Gallium-Catalyzed Electrochemical Reduction of $CO_2$ to Highly Reduced Products at Low Overpotentials. *ACS Catal.* **2016**, *6*, 2100−2104.
(27) Bagger, A.; Ju, W.; Varela, A. S.; Strasser, P.; Rossmeisl, J. Electrochemical $CO_2$ Reduction: A Classification Problem. *ChemPhysChem* **2017**, *18*, 3266−3273.
(28) Kortlever, R.; Peters, I.; Balemans, C.; Kas, R.; Kwon, Y.; Mul, G.; Koper, M. T. M. Palladium-Gold Catalyst for the Electrochemical Reduction of $CO_2$ to $C_1$-$C_5$ Hydrocarbons. *Chem. Commun.* **2016**, *52*, 10229−10232.
(29) Peterson, A. A.; Abild-Pedersen, F.; Studt, F.; Rossmeisl, J.; Nørskov, J. K. How Copper Catalyzes the Electroreduction of $CO_2$ into Hydrocarbon Fuels. *Energy Environ. Sci.* **2010**, *3*, 1311−1315.
(30) Schouten, K. J. P.; Qin, Z.; Pérez Gallent, E.; Koper, M. T. M. Two Pathways for the Formation of Ethylene in CO Reduction on Single-Crystal Copper Electrodes. *J. Am. Chem. Soc.* **2012**, *134*, 9864−9867.
(31) Calle-Vallejo, F.; Koper, M. T. M. Theoretical Considerations on the Electroreduction of CO to $C_2$ Species on Cu(100) Electrodes. *Angew. Chem., Int. Ed.* **2013**, *52*, 7282−7285.
(32) Huang, Y.; Handoko, A. D.; Hirunsit, P.; Yeo, B. S. Electrochemical Reduction of $CO_2$ Using Copper Single-Crystal Surfaces: Effects of CO* Coverage on the Selective Formation of Ethylene. *ACS Catal.* **2017**, *7*, 1749−1756.
(33) Hahn, C.; Hatsukade, T.; Kim, Y.-G.; Vailionis, A.; Baricuatro, J. H.; Higgins, D. C.; Nitopi, S. A.; Soriaga, M. P.; Jaramillo, T. F. Engineering Cu Surfaces for the Electrocatalytic Conversion of $CO_2$: Controlling Selectivity toward Oxygenates and Hydrocarbons. *Proc. Natl. Acad. Sci. U. S. A.* **2017**, *114*, 5918−5923.
(34) Klinkova, A.; De Luna, P.; Dinh, C.-T.; Voznyy, O.; Larin, E. M.; Kumacheva, E.; Sargent, E. H. Rational Design of Efficient Palladium Catalysts for Electroreduction of $CO_2$ to Formate. *ACS Catal.* **2016**, *6*, 8115−8120.
(35) Liu, S.; Tao, H.; Zeng, L.; Liu, Q.; Xu, Z.; Liu, Q.; Luo, J.-L. Shape-Dependent Electrocatalytic Reduction of $CO_2$ to CO on Triangular Silver Nanoplates. *J. Am. Chem. Soc.* **2017**, *139*, 2160−2163.
(36) Lee, H.-E.; Yang, K. D.; Yoon, S. M.; Ahn, H.-Y.; Lee, Y. Y.; Chang, H.; Jeong, D. H.; Lee, Y.-S.; Kim, M. Y.; Nam, K. T. Concave Rhombic Dodecahedral Au Nanocatalyst with Multiple High-Index Facets for $CO_2$ Reduction. *ACS Nano* **2015**, *9*, 8384−8393.
(37) Roberts, F. S.; Kuhl, K. P.; Nilsson, A. High Selectivity for Ethylene from $CO_2$ Reduction over Copper Nanocube Electrocatalysts. *Angew. Chem., Int. Ed.* **2015**, *54*, 5179−5182.
(38) Gao, D.; Zegkinoglou, I.; Divins, N. J.; Scholten, F.; Sinev, I.; Grosse, P.; Roldan Cuenya, B. Plasma-Activated Copper Nanocube Catalysts for Efficient $CO_2$ Electroreduction to Hydrocarbons and Alcohols. *ACS Nano* **2017**, *11*, 4825−4831.
(39) Grosse, P.; Gao, D.; Scholten, F.; Sinev, I.; Mistry, H.; Roldan Cuenya, B. Dynamic Changes in the Structure, Chemical State and Catalytic Selectivity of Cu Nanocubes during $CO_2$ Electroreduction: Size and Support Effects. *Angew. Chem., Int. Ed.* **2018**, *57*, 6192−6197.
(40) Baturina, O.; Lu, Q.; Xu, F.; Purdy, A.; Dyatkin, B.; Sang, X.; Unocic, R.; Brintlinger, T.; Gogotsi, Y. Effect of Nanostructured Carbon Support on Copper Electrocatalytic Activity toward $CO_2$ Electroreduction to Hydrocarbon Fuels. *Catal. Today* **2017**, *288*, 2−10.
(41) Gao, D.; Zhang, Y.; Zhou, Z.; Cai, F.; Zhao, X.; Huang, W.; Li, Y.; Zhu, J.; Liu, P.; Yang, F.; Wang, G.; Bao, X. Enhancing $CO_2$ Electroreduction with the Metal−Oxide Interface. *J. Am. Chem. Soc.* **2017**, *139*, 5652−5655.
(42) Jeon, H. S.; Kunze, S.; Scholten, F.; Roldan Cuenya, B. Prism-Shaped Cu Nanocatalysts for Electrochemical $CO_2$ Reduction to Ethylene. *ACS Catal.* **2018**, *8*, 531−535.
(43) Mariano, R. G.; McKelvey, K.; White, H. S.; Kanan, M. W. Selective Increase in $CO_2$ Electroreduction Activity at Grain-Boundary Surface Terminations. *Science* **2017**, *358*, 1187−1192.


DOI: 10.1021/acs.accounts.8b00360
*Acc. Chem. Res.* 2018, 51, 2906−2917

(44) Dutta, A.; Rahaman, M.; Luedi, N. C.; Mohos, M.; Broekmann, P. Morphology Matters: Tuning the Product Distribution of $CO_2$ Electroreduction on Oxide-Derived Cu Foam Catalysts. *ACS Catal.* **2016**, *6*, 3804−3814.
(45) Mistry, H.; Varela, A. S.; Bonifacio, C. S.; Zegkinoglou, I.; Sinev, I.; Choi, Y. W.; Kisslinger, K.; Stach, E. A.; Yang, J. C.; Strasser, P.; Roldan Cuenya, B. Highly Selective Plasma-Activated Copper Catalysts for $CO_2$ Reduction to Ethylene. *Nat. Commun.* **2016**, *7*, 12123.
(46) Li, C. W.; Kanan, M. W. $CO_2$ Reduction at Low Overpotential on Cu Electrodes Resulting from the Reduction of Thick $Cu_2O$ Films. *J. Am. Chem. Soc.* **2012**, *134*, 7231−7234.
(47) Tang, W.; Peterson, A. A.; Varela, A. S.; Jovanov, Z. P.; Bech, L.; Durand, W. J.; Dahl, S.; Nørskov, J. K.; Chorkendorff, I. The Importance of Surface Morphology in Controlling the Selectivity of Polycrystalline Copper for $CO_2$ Electroreduction. *Phys. Chem. Chem. Phys.* **2012**, *14*, 76−81.
(48) Chen, Y.; Li, C. W.; Kanan, M. W. Aqueous $CO_2$ Reduction at Very Low Overpotential on Oxide-Derived Au Nanoparticles. *J. Am. Chem. Soc.* **2012**, *134*, 19969−19972.
(49) Mistry, H.; Choi, Y.-W.; Bagger, A.; Scholten, F.; Bonifacio, C. S.; Sinev, I.; Divins, N. J.; Zegkinoglou, I.; Jeon, H.; Kisslinger, K.; Stach, E. A.; Yang, J. C.; Rossmeisl, J.; Roldan Cuenya, B. Enhanced $CO_2$ Electroreduction to CO over Defect-Rich Plasma-Activated Silver Catalysts. *Angew. Chem., Int. Ed.* **2017**, *56*, 11394−11398.
(50) Pander, J. E.; Ren, D.; Huang, Y.; Loo, N. W. X.; Hong, S. H. L.; Yeo, B. S. Understanding the Heterogeneous Electrocatalytic Reduction of $CO_2$ on Oxide-Derived Catalysts. *ChemElectroChem* **2018**, *5*, 219−237.
(51) Favaro, M.; Xiao, H.; Cheng, T.; Goddard, W. A.; Yano, J.; Crumlin, E. J. Subsurface Oxide Plays a Critical Role in $CO_2$ Activation by Cu(111) Surfaces to Form Chemisorbed $CO_2$, the First Step in Reduction of $CO_2$. *Proc. Natl. Acad. Sci. U. S. A.* **2017**, *114*, 6706−6711.
(52) Le Duff, C. S.; Lawrence, M. J.; Rodriguez, P. Role of the Adsorbed Oxygen Species in the Selective Electrochemical Reduction of $CO_2$ to Alcohols and Carbonyls on Copper Electrodes. *Angew. Chem., Int. Ed.* **2017**, *56*, 12919−12924.
(53) Ren, D.; Deng, Y.; Handoko, A. D.; Chen, C. S.; Malkhandi, S.; Yeo, B. S. Selective Electrochemical Reduction of $CO_2$ to Ethylene and Ethanol on Copper(I) Oxide Catalysts. *ACS Catal.* **2015**, *5*, 2814−2821.
(54) Zhou, Y.; Che, F.; Liu, M.; Zou, C.; Liang, Z.; De Luna, P.; Yuan, H.; Li, J.; Wang, Z.; Xie, H.; Li, H.; Chen, P.; Bladt, E.; Quintero-Bermudez, R.; Sham, T.-K.; Bals, S.; Hofkens, J.; Sinton, D.; Chen, G.; Sargent, E. H. Dopant-Induced Electron Localization Drives $CO_2$ Reduction to $C_2$ Hydrocarbons. *Nat. Chem.* **2018**, *10*, 974−980.
(55) Zhang, Y. J.; Peterson, A. Oxygen-Induced Changes to Selectivity-Determining Steps in Electrocatalytic $CO_2$ Reduction. *Phys. Chem. Chem. Phys.* **2015**, *17*, 4505−4515.
(56) Kim, D.; Lee, S.; Ocon, J. D.; Jeong, B.; Lee, J. K.; Lee, J. Insights into an Autonomously Formed Oxygen-Evacuated $Cu_2O$ Electrode for the Selective Production of $C_2H_4$ from $CO_2$. *Phys. Chem. Chem. Phys.* **2015**, *17*, 824−830.
(57) Xiao, H.; Goddard, W.; Cheng, T.; Liu, Y. Cu Metal Embedded in Oxidized Matrix Catalyst to Promote $CO_2$ Activation and CO Dimerization for Electrochemical Reduction of $CO_2$. *Proc. Natl. Acad. Sci. U. S. A.* **2017**, *114*, 6685−6688.
(58) Garza, A. J.; Bell, A. T.; Head-Gordon, M. Is Subsurface Oxygen Necessary for the Electrochemical Reduction of $CO_2$ on Copper? *J. Phys. Chem. Lett.* **2018**, *9*, 601−606.
(59) Wang, S.; Wang, J.; Xin, H. Insights into Electrochemical $CO_2$ Reduction on Tin Oxides from First-Principles Calculations. *Green Energy Environ.* **2017**, *2*, 168−171.
(60) Chen, Y.; Kanan, M. W. Tin Oxide Dependence of the $CO_2$ Reduction Efficiency on Tin Electrodes and Enhanced Activity for Tin/Tin Oxide Thin-Film Catalysts. *J. Am. Chem. Soc.* **2012**, *134*, 1986−1989.
(61) Dutta, A.; Kuzume, A.; Rahaman, M.; Vesztergom, S.; Broekmann, P. Monitoring the Chemical State of Catalysts for $CO_2$ Electroreduction: An In Operando Study. *ACS Catal.* **2015**, *5*, 7498−7502.
(62) Singh, M. R.; Kwon, Y.; Lum, Y.; Ager, J. W.; Bell, A. T. Hydrolysis of Electrolyte Cations Enhances the Electrochemical Reduction of $CO_2$ over Ag and Cu. *J. Am. Chem. Soc.* **2016**, *138*, 13006−13012.
(63) Lum, Y.; Yue, B.; Lobaccaro, P.; Bell, A. T.; Ager, J. W. Optimizing C-C Coupling on Oxide-Derived Copper Catalysts for Electrochemical $CO_2$ Reduction. *J. Phys. Chem. C* **2017**, *121*, 14191−14203.
(64) Pérez-Gallent, E.; Marcandalli, G.; Figueiredo, M. C.; Calle-Vallejo, F.; Koper, M. T. M. Structure- and Potential-Dependent Cation Effects on CO Reduction at Copper Single-Crystal Electrodes. *J. Am. Chem. Soc.* **2017**, *139*, 16412−16419.
(65) Dunwell, M.; Lu, Q.; Heyes, J. M.; Rosen, J.; Chen, J. G.; Yan, Y.; Jiao, F.; Xu, B. The Central Role of Bicarbonate in the Electrochemical Reduction of $CO_2$ on Gold. *J. Am. Chem. Soc.* **2017**, *139*, 3774−3783.
(66) Zhu, S.; Jiang, B.; Cai, W.-B.; Shao, M. Direct Observation on Reaction Intermediates and the Role of Bicarbonate Anions in $CO_2$ Electrochemical Reduction Reaction on Cu Surfaces. *J. Am. Chem. Soc.* **2017**, *139*, 15664−15667.
(67) Wuttig, A.; Yoon, Y.; Ryu, J.; Surendranath, Y. Bicarbonate Is Not a General Acid in Au-Catalyzed $CO_2$ Electroreduction. *J. Am. Chem. Soc.* **2017**, *139*, 17109−17113.
(68) Schouten, K. J. P.; Pérez Gallent, E.; Koper, M. T. M. The Influence of pH on the Reduction of CO and $CO_2$ to Hydrocarbons on Copper Electrodes. *J. Electroanal. Chem.* **2014**, *716*, 53−57.
(69) Dinh, C.; Burdyny, T.; Kibria, G.; Seifitokaldani, A.; Christine, M.; et al. $CO_2$ Electroreduction to Ethylene via Hydroxide-Mediated Copper Catalysis at an Abrupt Interface. *Science* **2018**, *360*, 783−787.
(70) Seifitokaldani, A.; Gabardo, C. M.; Burdyny, T.; Dinh, C.-T.; Edwards, J. P.; Kibria, M. G.; Bushuyev, O. S.; Kelley, S. O.; Sinton, D.; Sargent, E. H. Hydronium-Induced Switching between $CO_2$ Electroreduction Pathways. *J. Am. Chem. Soc.* **2018**, *140*, 3833−3837.
(71) Gao, D.; Scholten, F.; Roldan Cuenya, B. Improved $CO_2$ Electroreduction Performance on Plasma-Activated Cu Catalysts via Electrolyte Design: Halide Effect. *ACS Catal.* **2017**, *7*, 5112−5120.
(72) Varela, A. S.; Ju, W.; Reier, T.; Strasser, P. Tuning the Catalytic Activity and Selectivity of Cu for $CO_2$ Electroreduction in the Presence of Halides. *ACS Catal.* **2016**, *6*, 2136−2144.
(73) Todoroki, M.; Hara, K.; Kudo, A.; Sakata, T. Electrochemical Reduction of High Pressure $CO_2$ at Pb, Hg and In Electrodes in an Aqueous $KHCO_3$ Solution. *J. Electroanal. Chem.* **1995**, *394*, 199−203.
(74) Melchaeva, O.; Voyame, P.; Bassetto, V. C.; Prokein, M.; Renner, M.; Weidner, E.; Petermann, M.; Battistel, A. Electrochemical Reduction of Protic Supercritical $CO_2$ on Copper Electrodes. *ChemSusChem* **2017**, *10*, 3660−3670.
(75) Rosen, B. A.; Salehi-Khojin, A.; Thorson, M. R.; Zhu, W.; Whipple, D. T.; Kenis, P. J. A.; Masel, R. I. Ionic Liquid−Mediated Selective Conversion of $CO_2$ to CO at Low Overpotentials. *Science* **2011**, *334*, 643−644.


DOI: 10.1021/acs.accounts.8b00360
*Acc. Chem. Res.* 2018, 51, 2906−2917